the FEBS Journal

Mapping contacts between regulatory domains of skeletal muscle TnC and TnI by analyses of single-chain chimeras

Ana O. Tiroli[1,2,*], Ljubica Tasic[1,*,†], Cristiano L. P. Oliveira[1,3], Carlos Bloch Jr[1,4], Iris Torriani[1,3], Chuck S. Farah[5] and Carlos H. I. Ramos[1,2]

1 Centro de Biologia Molecular Estrutural, Laboratório Nacional de Luz Síncrotron, Brazil
2 Departamento de Bioquímica, Instituto de Biologia, Universidade Estadual de Campinas, Brazil
3 Instituto de Física, Universidade Estadual de Campinas, Brazil
4 Laboratório de Espectrometria de Massa, Embrapa-Recursos Genéticos e Biotecnologia, Brazil
5 Departamento de Bioquímica, Instituto de Química, Universidade de São Paulo, Brazil

Keywords
troponin; muscle contraction; protein engineering; limited proteolysis; solution structure

Correspondence
C.H.I. Ramos, Centro de Biologia Molecular Estrutural, Laboratório Nacional de Luz Síncrotron, CP 6192, Campinas SP, 13084-971 Brazil
Fax: +55 19 3287 7110
Tel: +55 19 3287 4520
E-mail: cramos@lnls.br

*These authors contributed equally to this work.

†Present address
Instituto de Química, Universidade Estadual de Campinas, Campinas SP, Brazil

(Received 19 October 2004, revised 24 November 2004, accepted 6 December 2004)

doi:10.1111/j.1742-4658.2004.04515.x

The troponin (Tn) complex is formed by TnC, TnI and TnT and is responsible for the calcium-dependent inhibition of muscle contraction. TnC and TnI interact in an antiparallel fashion in which the N domain of TnC binds in a calcium-dependent manner to the C domain of TnI, releasing the inhibitory effect of the latter on the actomyosin interaction. While the crystal structure of the core cardiac muscle troponin complex has been determined, very little high resolution information is available regarding the skeletal muscle TnI–TnC complex. With the aim of obtaining structural information regarding specific contacts between skeletal muscle TnC and TnI regulatory domains, we have constructed two recombinant chimeric proteins composed of the residues 1–91 of TnC linked to residues 98–182 or 98–147 of TnI. The polypeptides were capable of binding to the thin filament in a calcium-dependent manner and to regulate the ATPase reaction of actomyosin. Small angle X-ray scattering results showed that these chimeras fold into compact structures in which the inhibitory plus the C domain of TnI, with the exception of residues 148–182, were in close contact with the N-terminal domain of TnC. CD and fluorescence analysis were consistent with the view that the last residues of TnI (148–182) are not well folded in the complex. MS analysis of fragments produced by limited trypsinolysis showed that the whole TnC N domain was resistant to proteolysis, both in the presence and in the absence of calcium. On the other hand the TnI inhibitory and C-terminal domains were completely digested by trypsin in the absence of calcium while the addition of calcium results in the protection of only residues 114–137.

Muscle contraction is regulated by the troponin (Tn) complex, which is composed of three subunits: TnC, TnI, and TnT [1,2]. TnC is the calcium binding subunit that possesses two Ca^{2+}-binding sites per domain [3,4]. TnI inhibits the actomyosin Mg^{2+}-ATPase in the presence of tropomyosin and inhibition is removed by TnC [5]. The inhibitory activity of TnI has been associated with a central peptide corresponding to residues 98–116, known as the inhibitory region [5].

Abbreviations
c, cardiac; GdmCl, guanidinium chloride; MM, molecular mass; SAXS, small angle X-ray scattering; TnC(1–91), N-terminus domain of TnC composed of residues 1–91; TnI(98–182), TnI inhibitory and C-terminal domains, residues 98–182; TnI(98–147), TnI(98–182) deleted of residues 148–182; TnC(1–91)–TnI(98–182), chimeric single-chain protein formed by TnC(1–91), a GGAGG linker and TnI(98–182); TnC(1–91)–TnI(98–147), chimeric single-chain protein formed by TnC(1–91), a GGAGG linker, and TnI(98–147); Tn, troponin.

TnC is dumbbell-shaped protein with two globular domains, each composed of two EF-hand calcium binding motifs, which are connected by an extended α-helix [6]. Under physiological conditions, the C-terminal domain is expected to be saturated with calcium ions, whereas calcium binding to the low-affinity sites at the N-terminal domain (residues 1–91) triggers muscle contraction [7]. The isolated N and C domains of TnC maintain their structural and functional characteristics [8] and calcium binding to N domain of TnC causes a conformational change that exposes a binding site for interaction with TnI [9]. The isolated domains of TnI were also investigated by studying N and C termini deletion mutants of TnI [10] showing that the C terminus of TnI (residues 117–182), when linked to the inhibitory region, has the major regulatory function of the molecule. The studies of isolated domains lead to the conclusions that the interaction between TnC and TnI is antiparallel [10], and that the inhibitory region and the region between residues 117 and 148 are involved in the binding to N domain of TnC [11–16]. Serial deletion studies of the C terminus of TnI showed that residues 166–182 are involved in binding to the thin filament [16]. Altogether, these studies showed that the TnC(1–91) and TnI(98–182) form a regulatory subunit, and that the first half of the C terminus of TnI is important for this binding.

Structural information of the interaction of TnC and TnI were firstly provided by low-resolution scattering studies [17,18] showing that the C terminus of TnI has a tubular-like conformation that involves the globular N domain of TnC. NMR studies have provided additional information on the structure of skeletal TnC(1–91) in the presence of TnI inhibitory peptide and residues 117–148 [19], and in the presence of TnI residues 115–131 [12]. However, high resolution information on the skeletal TnI(98–182) in solution has proven difficult to obtain. Recently, Takeda *et al.* [20] presented the high-resolution structure of the calcium-saturated human cTn. Although this structural resolution took us a step closer to understanding the action of troponin, some portions of the inhibitory and C-terminal domains of TnI are lacking in this model and more structural information is necessary for full comprehension of Tn function.

To investigate the interactions between skeletal muscle TnC(1–91) and TnI(98–182), we have constructed two single chain chimeras composed of these domains. The chimeras were formed by residues 1–91 of TnC and residues 98–182 or 98–147 of TnI, connected by a GlyGlyAlaGlyGly linker. The obligatory 1 : 1 TnC/TnI stoichiometry provided by these single-chain chimeras facilitated their conformational analysis by a variety of methods including SAXS, MS and proteolysis.

Results

Expression, purification, and initial conformational analyses

The chimeric gene encodes a single chain polypeptide that has residues 1–91 of TnC in its N terminus, a GGAGG linker, and then residues 98–182 of TnI for TnC(1–91)–TnI(98–182) or 98–147 for TnC(1–91)–TnI(98–147) (Fig. 1A). The two chimeras were expressed in *Escherichia coli* and purified in soluble state (Fig. 1B). The purified chimeras showed no sign

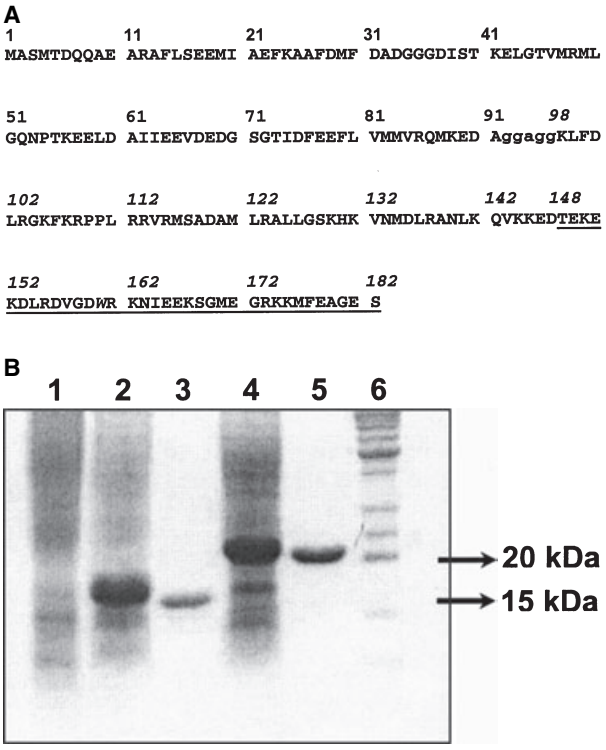

Fig. 1. (A) Amino acid sequence of the chimeras TnC(1–91)–TnI(98–182) and TnC(1–91)–TnI(98–147). The chimeras are composed from TnC residues 1–91, followed by a GGAGG linker followed by residues 98–182 or 98–147 of TnI. The GGAGG linker is shown in lowercase and the Trp residue is shown in italic. The TnI sequence that is deleted in the chimera TnC(1–91)–TnI(98–147) is shown underlined. (B) SDS/PAGE 15%. Lane 1, bacterial pellet before induction; lane 2, bacterial pellet of TnC(1–91)–TnI(98–182) after 4 h of induction; lane 3, TnC(1–91)–TnI(98–182) after purification; lane 4, bacterial pellet of TnC(1–91)–TnI(98–147) after 4 h of induction; lane 5, TnC(1–91)–TnI(98–147) after purification; lane 6, Molecular mass markers.

of impurities or degradation, were soluble even in pure water and folded (see below). The folded state of the two chimeras was investigated by CD spectroscopy (Fig. 2A and Table 1). The CD spectra of the two chimeras were very similar (Fig. 2A) and did not vary significantly upon the addition of calcium (data not shown). TnI has a Trp residue at position 160 that is maintained in the chimera TnC(1–91)–TnI(98–182) and emission fluorescence spectroscopy was used to observe the environment of this residue. The emission fluorescence spectrum indicated that the W160 was exposed to the solvent as confirmed by the maximum intensity wavelength of 343 nm and emission fluorescence centre of mass at 351 nm (Fig. 2B and Table 1). There were no relevant differences in the emission fluorescence spectra of TnC(1–91)–TnI(98–182) in the absence or in the presence of calcium (Table 1), and the addition of the denaturant guanidinium chloride (GdmCl) caused only a very small red shift in the emission spectrum (Fig. 2B and Table 1).

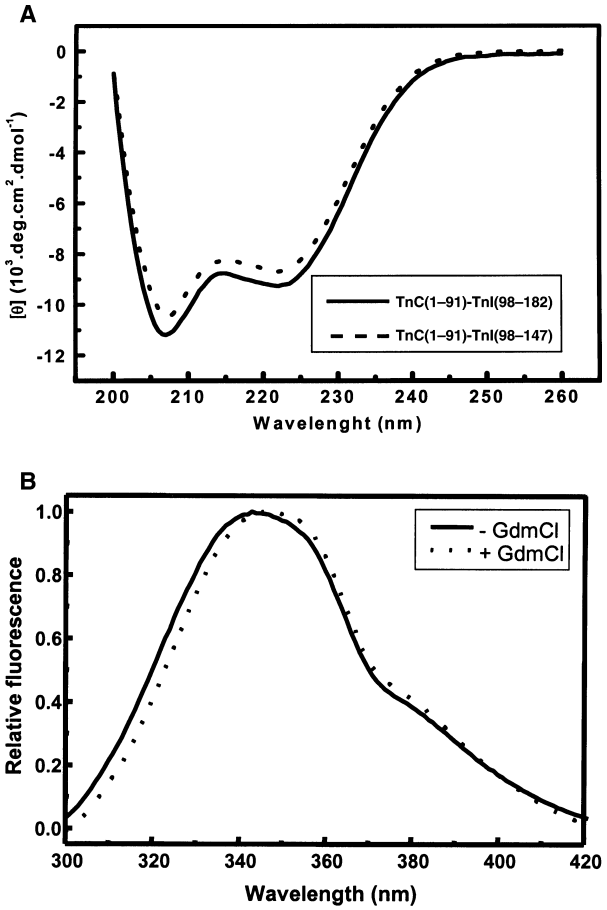

Fig. 2. (A) CD spectra of TnC(1–91)–TnI(98–182) (solid line) and of TnC(1–91)–TnI(98–147) (dashed line). The spectra in the presence or in the absence of calcium are indistinguishable (data not shown). The spectra of TnC(1–91)–TnI(98–182) and TnC(1–91)–TnI(98–147) are characteristic of α-helical proteins. (B) Fluorescence spectra of TnC(1–91)–TnI(98–182) in the absence (solid line) and in the presence (dashed line) of GdmCl. The fluorescence spectrum of TnC(1–91)–TnI(98–182) is characteristic of a solvent exposed tryptophan.

Functional analyses

The functional characteristics of the chimeras were analysed by cosedimentation with actin and tropomyosin followed by SDS/PAGE, and by their ability to regulate the ATPase activity of actomyosin. Both experiments were performed in the absence and in the presence of calcium and the results are described in Table 1. The TnC(1–91)–TnI(98–182) chimera cosedimented with actin–tropomyosin and inhibited about 48% of the actomyosin ATPase activity in the absence of calcium (Table 1). In the presence of calcium, TnC(1–91)–TnI(98–182) did not cosediment with actin–tropomyosin and did not inhibit the ATPase activity of actomyosin (Table 1). In the absence of calcium, the TnC(1–91)–TnI(98–147) chimera had a lower cosedimentation with actin–tropomyosin when compared to TnC(1–91)–TnI(98–182) and inhibited about 35% of the actomyosin ATPase activity (Table 1). TnC(1–91)–TnI(98–147) did not inhibit the actomyosin ATPase activity nor did it cosediment with actin–tropomyosin in the presence of calcium. These results indicated that the chimeras presented functional properties similar to that of the TnC–TnI complex [10].

Limited proteolysis and MS analyses

The tryptic peptides generated by the lysis of TnC(1–91)–TnI(98–147) with trypsin were analysed by MS (Fig. 3). No peptides from the TnC(1–91) portion were released in the presence or in the absence of calcium not even after 24 h incubation at 37 °C, confirming the high stability of this domain [21]. The TnI(98–147) portion was completely digested even at 4 °C in the absence of calcium and peptides corresponding to regions 99–103 ($m/z = 664$, LFDLR), 108–112 ($m/z = 639$, RPPLR), 116–123 ($m/z = 895$, MSADAMLR), 124–129 ($m/z = 589$, ALLGSK), 132–137 ($m/z = 747$, VNMDLR), and 138–141 ($m/z = 445$, ANLK) were identified (Fig. 3A,B). When the trypsinolysis reaction was performed in the presence of calcium, the following peptides derived from the TnI(98–147) portion of the chimera, 116–123 ($m/z = 895$, MSADAMLR), 124–129 ($m/z = 589$, ALLGSK), and 132–137 ($m/z = 747$, VNMDLR), were not identified even after up to 45 min of reaction. Instead, a molecular ion ($m/z = 2712$) that corresponds to the region 114–137 (VRMSADAMLRALLGSKHKVNMDLR) was

Table 1. Chimeras biophysical and functional parameters. The errors are < 4%.

	TnC(1–91)–TnI(98–182) (– calcium)	TnC(1–91)–TnI(98–182) (+ calcium)	TnC(1–91)–TnI(98–147) (– calcium)	TnC(1–91)–TnI(98–147) (+ calcium)
CD at 222 nm ($deg.cm^{-2}·dmol^{-1}$)	–9300	–9450	–8800	–8850
Emission fluorescence λ_{Max} [a] (nm)	343	343	–	–
Emission fluorescence Mass centre[a] (nm)	351	351	–	–
Bind to the thin filament[b]	++	No	+	No
Actomyosin ATPase activity (%)	52[c]	100	65[c]	100
Radius of gyration[d] (Å)	30	30	23	23

[a] In the presence of GdmCl, λ_{Max} = 347 nm and mass centre = 353 nm. [b] ++, Strong binding; + weak binding [16]. [c] The actomyosin ATPase activity in the presence of the binary complex formed by TnI and TnC and in the absence of calcium is 40% [10,16]. [d] Measured by SAXS.

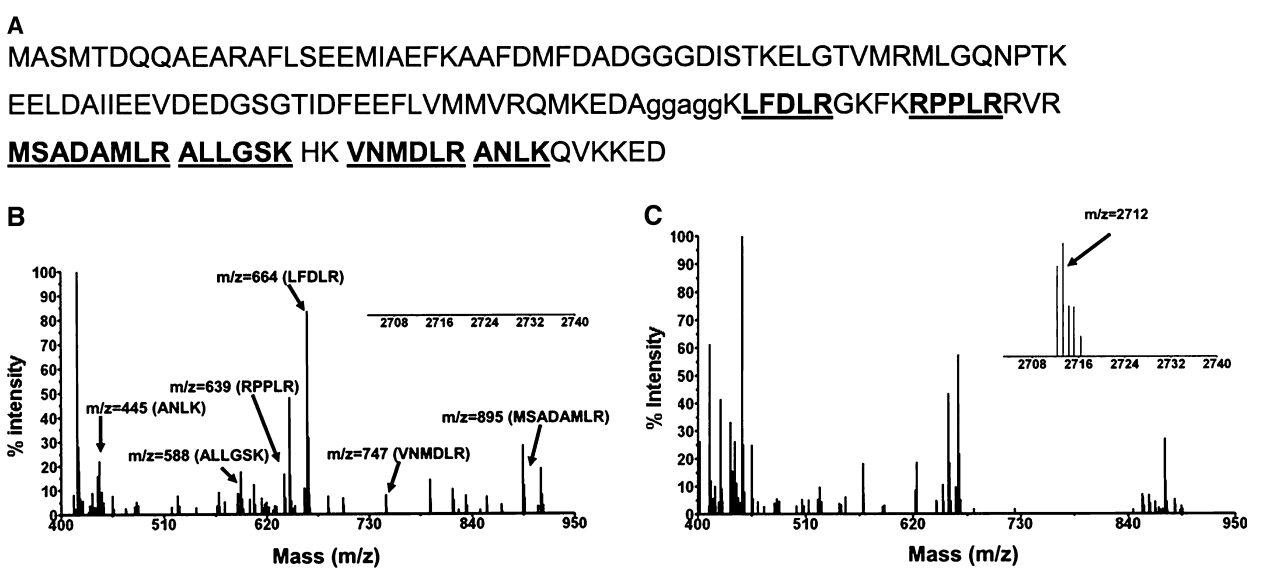

Fig. 3. (A) Amino acid sequence of TnC(1–91)–TnI(98–147) showing in bold the fragments that were digested with trypsin in the absence of calcium. (B) Mass spectra of digested TnC(1–91)–TnI(98–147) apo protein after 15 min treatment with trypsin at 4 °C. The peptic fragments identified by MALDI-TOF-MS were: 99–103 (m/z = 664, LFDLR), 108–112 (m/z = 639, RPPLR), 116–123 (m/z = 895, MSADAMLR), 124–129 (m/z = 588, ALLGSK), 132–137 (m/z = 747, VNMDLR) and 138–141 (m/z = 445, ANLK). (C) Mass spectrum of digested holo protein after 15-min treatment with trypsin at 4 °C. A peptide corresponding to residues 114–137 (m/z = 2712, VRMSADAMLRALLG SKHKVNMDLR) was identified. Therefore, the peptides 116–123 (m/z = 895, MSADAMLR), 124–129 (m/z = 589, ALLGSK) and 132–137 (m/z = 747, VNMDLR) were protected from trypsin digestion in the presence of calcium.

observed (Fig. 3C). However, after 60 min of lysis, the large fragment was no longer present and the smaller peptides appeared (data not shown). The chimera TnC(1–91)–TnI(98–182) had the same behaviour as the chimera TnC(1–91)–TnI(98–147).

Small angle X-ray scattering experiments

SAXS measurements were performed for TnC(1–91), TnC(1–91)–TnI(98–182), and TnC(1–91)–TnI(98–147). The experiments were performed in the presence and in the absence of calcium, which gave undistinguishable results (Table 1). The experimental intensity data as a function of the modulus of the scattering vector q are shown for TnC(1–91)–TnI(98–182) (Fig. 4A) and TnC(1–91)–TnI(98–147) (Fig. 4B). The value of the radius of gyration obtained for TnC(1–91)–TnI(98–182) was 30 ± 2 Å with a maximum dimension of ≈110 Å (Fig. 4A and Table 1). For the protein TnC(1–91)–TnI(98–147) the calculated

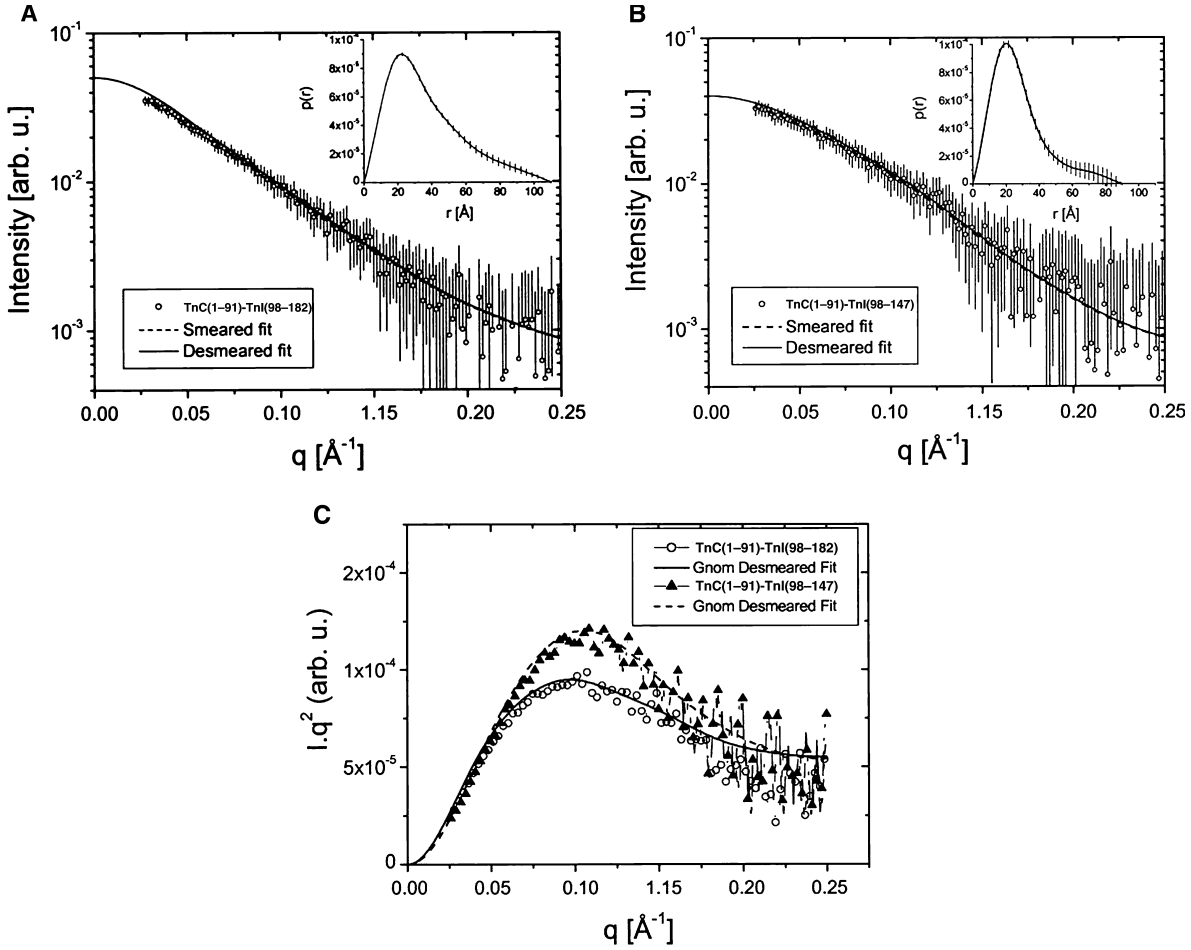

Fig. 4. (A) TnC(1–91)–TnI(98–182) experimental data and GNOM fitting. Inset: pair distance distribution function p(r). The experimental values for D_{max} and R_g, 110 Å and 30 Å, respectively, suggest that the protein is elongated. (B) TnC(1–91)–TnI(98–147) experimental data and GNOM fitting. Inset: pair distance distribution function p(r). D_{max} and R_g, 90 Å and 23 Å, respectively, suggest that this protein is also elongated but smaller than TnC(1–91)–TnI(98–182). (C) Kratky plots for both proteins. This plot suggests that the proteins have flexible chains in solution.

radius of gyration was 23 ± 2 Å and the maximum dimension ≈90 Å (Fig. 4B and Table 1). As expected, the chimera TnC(1–91)–TnI(98–147) was smaller than the chimera TnC(1–91)–TnI(98–182). In both cases the p(r) function indicated an elongated (prolate) shape for the protein conformation. The general behaviour for the p(r) function was similar for the two proteins, and the major differences occur for large *r*-values. The differences in size and radius of gyration indicated that the portion missing in the chimera TnC(1–91)–TnI(98–147) did not occupy a central part in the structure of protein TnC(1–91)–TnI(98–182), but was probably located near one of the extremities. As showed in Fig. 4C, the Kratky plots suggested the presence of some flexible domains for both TnC(1–91)–TnI(98–182) and TnC(1–91)–TnI(98–147). Due to the large homology between the sequences of these chimeras, we also expected a marked similarity in the structures. This was partially indicated by the general shape of the p(r) functions (Fig. 4A,B), where the maximum of the curves had approximately the same value in both cases and by the Kratky plot that showed similarity in the flexibility of the structures of the two proteins (Fig. 4C).

SAXS modelling

The Fig. 5A shows the high-resolution structure of the TnC(1–91) (1SKT) as well as an *ab initio* model calculated from SAXS experimental data of the TnC(1–91) protein in solution. Ten independent models were averaged using the GASBOR program, which uses the same principles as the CHADD program but the simulated dummy backbone corresponds to the whole protein. This additional experiment and the corresponding

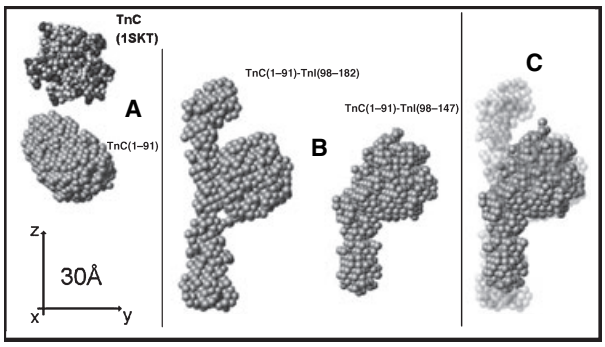

Fig. 5. (A) High-resolution structure of the TnC(1–91) (1SKT) as well as an *ab initio* model calculated from SAXS experimental data of the protein in solution. The low-resolution structure of the TnC(1–91) corresponded to its high-resolution structure. (B) The models correspond to the most probable solution structure obtained for TnC(1–91)–TnI(98–182) and TnC(1–91)–TnI(98–147) from the averaging process using spheres with packing radius of 1.5 Å. Both models had prolate conformation and the position of the TnC(1–91) and TnI(98–182) were located. (C) The models of TnC(1–91)–TnI(98–182) (semitransparent spheres) and TnC(1–91)–TnI(98–147) (solid spheres) were superimposed. From this comparison it was easy to locate the portion corresponding to residues 148–182 of TnI.

calculation were carried out to confirm that the crystallographic structure of the TnC(1–91) corresponded to its high-resolution structure. The correspondence was also confirmed by the perfect fit of the TnC(1–91) experimental data using the program CRYSOL [22] with the TnC(1–91) NMR structure (1SKT) as an input to this program. The models shown in Fig. 5B correspond to the most probable solution structure obtained for TnC(1–91)–TnI(98–182) and TnC(1–91)–TnI(98–147) from the averaging process using spheres with packing radius of 1.5 Å. Both models had prolate conformations and the positions of TnC(1–91) and TnI(98–182) were located. To compare the models, they were superimposed as shown in Fig. 5C. The semitransparent spheres correspond to the most probable model configuration for TnC(1–91)–TnI(98–182) and the solid spheres to TnC(1–91)–TnI(98–147). From this comparison the deleted portion of TnI becomes apparent. Finally, from the superimposed models presented in Fig. 5 we observe that: (a) the globular part represents the TnC(1–91); (b) the tube-like structure extending from the globule common to both chimeras, represents the TnI(98-147) component; and (c) the second tube-like structure that is present only in TnC(1–91)–TnI(98–182) represents the region 148–182 of TnI.

As a final check of the model building from SAXS data, we performed hydrodynamic calculations using the program HYDROPRO to obtain the volume of the models [23,24]. It is interesting to compare the pairs of ratios: (a) V[model-TnC(1–91)–TnI(98–182)]/V(1SKT) and MM[TnC(1–91)–TnI(98–182)]/MM(1SKT); (b) V[model-TnC(1–91)–TnI(98–147)]/V(1SKT) and MM [TnC(1–91)–TnI(98–147)]/MM(1SKT); and (c) V[model-TnC(1–91)–TnI(98–182)]/V(model-TnC(1–91)–TnI(98–147)] and MM[TnC(1–91)–TnI(98–182)]/MM[TnC (1–91)–TnI(98–147)]. If the modelling is correct, these ratios should give similar values. The hydrodynamic calculations for the models were performed using a subunit radius of 5.36 Å. This value was estimated so that the CA backbone model will furnish the correct hydrodynamic values of the real protein. For the calculation of the TnC(1–91) (1SKT) hydrodynamic values we used a subunit radius of 3.1 Å as recommended in the HYDROPRO program. Table 2 lists the above ratios and shows that we find similar values for all the structures compared, indicating that the models correctly retrieve the volume ratios.

Discussion

The chimeras were folded and functional

Protein engineering the connection of two or more protein units to create a single polypeptide chain is a powerful alternative model to investigate the protein characteristics. Among the diverse past examples of the application of this approach are the linking of monomers into dimers [25], the identification of essential functional regions in homologous proteins [26], the production of attached protein-reporters to facilitate purification or the investigation of activity [27], the creation of antibody chimeras [28], and the study of

Table 2. The ratios of the volumes (V) of the models built by SAXS and of the structure of TnC(1–91) (1SKT) are compared with their molecular mass (MM) ratios.

Volume comparison		Molecular mass comparison	
V[model-TnC(1–91)–TnI(98–182)]/V(1SKT)	2.0 ± 0.2	MM[TnC(1–91)–TnI(98–182)]/MM(1SKT)	2.0
V[model-TnC(1–91)–TnI(98–147)]/V(1SKT)	1.6 ± 0.2	MM[TnC(1–91)–TnI(98–147)]/MM(1SKT)	1.6
V[model-TnC(1–91)–TnI(98–182)]/V (model-TnC(1–91)–TnI(98–147)	1.3 ± 0.1	MM[TnC(1–91)–TnI(98–182)]/MM[TnC(1–91)–TnI(98–147)]	1.3

protein–protein interactions [29,30]. The study of TnI separated from other components of the Tn complex has always been difficult due to its low solubility, which increases only in the presence of the TnC. In order to improve the solubility of TnI and to guarantee a 1 : 1 stoichiometry of TnI/TnC we created two single chain chimeras that mimic the regulatory domain of the TnI–TnC binary complex.

CD analysis of the purified chimeric proteins indicated that they fold into predominantly α-helical conformations. TnC and the residues corresponding to the skeletal TnI 117–160 in cTnI have high α-helical content [6,20]. The chimeras had functional similarity with the experiments performed with truncated TnC(1–91) and TnI(98–182) or TnI(1–147) not covalently connected by peptide bond [10,16]. The TnC(1–91)–TnI(98–182) chimera was able to bind and to regulate the actomyosin ATPase activity in a manner similar to the TnC–TnI complex. The TnC(1–91)–TnI(98–147) chimera showed lower binding affinity as well as lower ability to regulate the actomyosin ATPase activity when compared to the larger chimera. These results are similar with the results observed for the binary complexes formed by TnC(1–91) and TnI(1–147), and TnC and TnI [16] and agree with the hypothesis that the entire C terminus of the TnI is important for the regulation of the actomyosin ATPase activity [10,16].

Defining the TnI region that binds to TnC(1–91)

Several studies have shown that the TnI region between residue 98 and residue 148 is involved in the interaction with the N domain of TnC upon calcium ion binding [10,15,16]. However, the true extension of this region, the residues involved, and the events that occur upon calcium binding are poorly defined. With the aim of mapping these subregions and the residues involved, we have created two chimera proteins that have single-chain, TnC(1–91) and TnI(98–182) or TnC(1–91) and TnI(98–147).

The compactness of the structures of TnC(1–91)–TnI(98–182) and TnC(1–91)–TnI(98–147) obtained from SAXS experiments are in agreement with a close localization of the N domain of TnC and the first half of the C terminus of TnI. The sensitivity to degradation by proteases is related to the conformational flexibility of the protein substrate [31], and we can assume that the VRMSADAMLRALLGSKHKVNMDLR region (114–137) of TnI interacts, in the presence of calcium, with the TnC_{1-91} fragment in a specific manner that protects it from digestion. There are several lines of evidence that this is the TnI region involved in the binding in the N domain of TnC. TnC can be cross-linked to residues 113–145 of TnI [11]. Pearlstone *et al*. [13] using a recombinant fragment of TnI containing residues 96–148 showed that residues 117–148 are responsible for binding the N domain of TnC. Takeda *et al*. [14] used limited proteolysis to show that residues 117–134 of TnI are involved in the binding of TnC in the presence of calcium. Tripet *et al*. [15] showed that mutations in the region 115–131 of TnI affects its binding to TnC. Ramos [16] showed that deletion mutants TnI(1–147) and TnI(1–136) exhibit similar binding to the N domain of TnC as wild-type TnI in the presence of calcium, however, further deletions [TnI(1–129) and TnI(1–116)] decrease this binding. Li *et al*. [32] used a cross-linking to show that the residue 117 of TnI is localized near the helices B and C of TnC in the presence of calcium and moves away from them when calcium is present. Recent work has demonstrated that the emission fluorescence of a probe at position 121 in TnI is sensitive to calcium binding to the N domain of TnC [33]. The crystal structure of cTn [20] showed that residues R117 to L128 of TnI (in chicken fast skeletal numbers) are in close contact with the N domain of TnC in the presence of calcium. These findings from other studies reinforce our observation that residues 114–137 are in fact involved in the interaction with calcium-loaded TnC.

Structural insights on the region comprising the last residues of TnI

Little is known about the structure of the last 20 residues in the C terminus of the TnI, probably because it lacks a rigid structure. The α-helical content was very similar for both chimeras and the emission fluorescence spectrum of Trp160 in TnC(1–91)–TnI(98–182) corresponds to the spectrum of a solvent exposed residue as shown for TnI by Lakowicz *et al*. [34], results which are probably due to the lack of a stable secondary structure in residues 148–182 of TnI. The comparison of the models generated by SAXS for TnC(1–91)–TnI(98–182) and TnC(1–91)–TnI(98–147) were informative about the position of the last residues (148–182) of the TnI. The chimera TnC(1–91)–TnI(98–182) had a large portion that was not in contact with TnC(1–91). Because this structure is lacking in the SAXS structure of TnC(1–91)–TnI(98–147), we can assume that this region corresponds to residues 148–182 of TnI. The last residues of cTnI are missing in the crystallographic structure [20] indication a badly folded or highly dynamic conformation in this region.

Therefore, the results obtained from CD, fluorescence, and SAXS indicated a model in which the last residues of TnI do not interact with TnC. We suggest

that the main function of this region is likely to be the binding to the thin filament and not to TnC. This hypothesis is in agreement with previous works. Takeda *et al*. [14] used limited proteolysis to show that residues 141–181 of TnI are involved in the binding to the thin filament. The deletion of the region comprising the last residues of TnI (166–182) decreases the inhibitory capacity of TnI [16]. Takeda *et al*. [20] showed that the residues G129–W160 (in chicken fast skeletal numbers) seem to be away from TnC. This structural arrangement would favour an interaction of residues 166–182 of TnI with the thin filament. When calcium is bound to TnC, the interaction with region 114–137 of TnI could facilitate the dissociation of region 166–182 of TnI from the thin filament.

Final comments

With the results presented in this work, combined with others available in the literature, we suggest a model for the structure of TnI and TnC that can explain how they interact during muscle contraction. Figure 6 shows a schematic representation of the structural disposition of TnC and TnI in the light of recent results from our group and others. The N terminus of TnI is displaced around the C domain of TnC [17,18,20]. The inhibitory region is positioned in a way that it can interact with both the N and the C domains of TnC (as suggested by the work of Farah *et al*. [10]). The region between residues 114 and 148 is localized near to the N domain of TnC and binds to it (this work). The region comprising the last residues of TnI is disposed away from TnC (this work) in such a way that facilitates its binding to the thin filament [16]. In this model (Fig. 6), the hydrophobic pocket opened upon calcium ion binding to the NTnC binds the residues 114–137 of TnI. This binding removes the inhibitory region and the last residues of TnI away from the thin filament allowing muscle contraction [5,10,16]. Crystallization experiments are in progress, and we hope that solving the structure at the atomic level of the chimeras studied here will lead to the identification of the functional domain of TnC and TnI, as well as complement the crystal structure of the entire troponin complex.

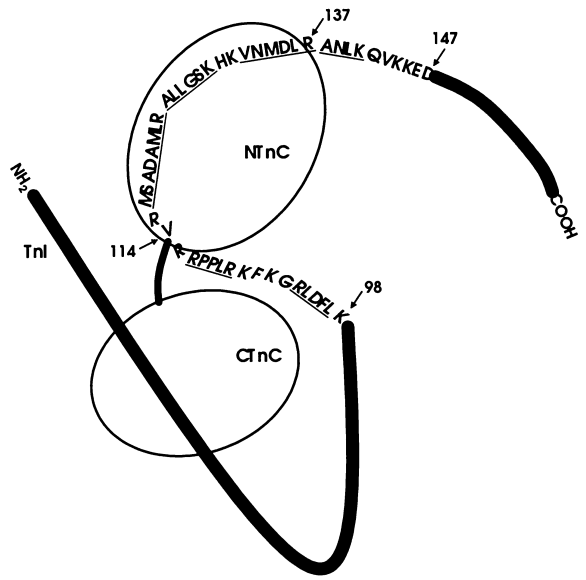

Fig. 6. Model structure of the interaction between TnC and TnI based on the SAXS model and in the tryptic peptides analyses in this work and on the information available in previous works. See Discussion for details.

Experimental procedures

Site-directed mutagenesis

The cDNAs of TnC and TnI were previously described [16] and the plasmid constructs for expression of the TnC–TnI chimeras were produced by PCR-based site-directed mutagenesis in two steps. For the first PCR using TnC cDNA template, the forward TnC oligo 5′-GATATACATAT GGCGTCA-3′ contains an *Nde*I site and an initiation codon and the reverse TnC oligo 5′-GCTCCTCCTCGCC GGCGCCCCCGGCGTCCTC-3′ contains the codons for the two glycines and one alanine plus an *Ngo*MIV restriction enzyme site placed after the Ala91 codon of TnC. For the second PCR, using the TnI cDNA template, the forward oligo 5′-GAGCTGGAGGACGCCGGCGGGAAG CTGTTTG-3′ contains an *Ngo*MIV restriction enzyme site plus the codons for two glycines before the codon for Lys98 of the TnI and the reverse TnI oligo 5′-CCCGG ATCCTTAGGACTCCCCGGCCTC-3′ contains a *Bam*HI restriction enzyme site after the stop codon, and can be used for either TnI and TnI(1–147) templates [16]. The PCR products were digested with *Ngo*MIV and ligated. This procedure resulted in the DNA sequence of TnC(1–91) connected to the DNA sequence of TnI(98–182) or TnI(98–147) by a nucleotide sequence coding for a GlyGlyAlaGlyGly linker. The PCR products, TnC(1–91)–TnI(98–182) and TnC(1–91)–TnI(98–147), were cloned into pET3a vector digested with *Nde*I and *Bam*HI creating the respective vectors pET3aTnC(1–91)–TnI(98–182) and pET3aTnC(1–91)–TnI(98–147). The constructs were confirmed by DNA sequencing.

Protein purification

The pET3aTnC(1–91)–TnI(98–182) and pET3aTnC(1–91)–TnI(98–147) vectors were transformed in *E. coli* strain

BL21(DE3)pLysS and expressed by adding 100 mM·L^{-1} of lactose at D_{600} = 0.8. The induced cells were grown overnight and harvested by centrifugation for 15 min at 2600 ***g***. The purification method was the same for both chimeric proteins. The bacterial pellet was suspended in 100 mM acetate buffer, pH 5.0, 8 M urea, 1 mM $CaCl_2$, and cells were lysed by French Press® followed by centrifugation for 15 min at 12 000 ***g***, 4 °C. The supernatant was ultracentrifuged for 60 min at 80 000 ***g*** at 4 °C in a Beckman TL100 ultracentrifuge, rotor TLA120.1 (Palo Alto, CA, USA) and a large amount of contaminants was precipitated. The supernatant of this step was dialysed overnight at 4 °C in the buffer described above without urea. After the dialyses, the suspension was centrifuged for 15 min at 12 000 ***g*** and 4 °C, and the soluble fraction was loaded into a DEAE–Sepharose column (Pharmacia, Uppsala, Sweden) equilibrated with 100 mM acetate buffer, pH 5.0, and 1 mM $CaCl_2$. The column was washed twice with the buffer, and then, a linear gradient of NaCl was applied. The TnC(1–91)–TnI(98–147) was eluted in the flow-through, while the TnC(1–91)–TnI(98–182) was eluted with 120 mM NaCl. The concentrations of the proteins were calculated by the BCA Protein Assay Kit (Pierce, Rockford, IL, USA). The production of TnC(1–91) was performed as previously described [16]. The calculated MS molecular masses were identical within the error margin to the expected molecular masses from the amino acid sequences of the chimeras [20363 for TnC(1–91)–TnI(98–182) and 16267 for TnC(1–91)–TnI(98–147)].

Spectroscopic experiments

CD measurements were taken using a Jasco J-810 spectropolarimeter (Tokyo, Japan) with temperature controlled by Peltier Type Control System PFD 4255. The CD spectra were taken in cuvettes of 1 cm pathlength using 4 μM protein in 0.5 mM Hepes buffer pH 7.0, 1 mM $CaCl_2$ for the experiments in the presence of calcium or 1 mM EDTA for the experiments in the absence of calcium at 20 °C. CD measurements were taken with scan speed of 50 nm·min^{-1} from 200 to 260 nm. Fluorescence measurements were made in an SLM AB2 spectrofluorimeter using a 1 × 1 cm pathlength cuvette, using the same conditions as in the CD experiments, with excitation at 280 nm and a bandpass of 8 nm, and emission at 320 nm with a bandpass of 8 nm. All spectra were baseline corrected with the buffer and were the means of at least three independent experiments.

ATPase activity and actin-binding experiments

The measurements of the actomyosin Mg^{2+}-ATPase activity and binding to actin were performed as previously described [10,16]. Briefly, actin (7 μM), tropomyosin (2 μM), myosin (0.4 μM), and chimeras (7 μM) were combined on ice in 25 mM Mops/HCl pH 7.0, 50 mM NaCl, 5 mM $MgCl_2$, 1 mM dithiothreitol, 1 mM EGTA for the experiments in the absence of calcium or 1 mM $CaCl_2$ for the experiments in the presence of calcium. ATP (2 mM) was added and the mixture incubated at 25 °C for 60 min, after which phosphate was determined [35]. Co-sedimentation experiments were performed using 7 μM actin, 2 μM tropomyosin, 7 μM chimera, diluted in 20 mM imidazole/HCl pH 7.0, 200 mM NaCl, 25 mM 2-mercaptoethanol, 1 mM EGTA for the experiments in the absence of calcium or 1 mM $CaCl_2$ for the experiments in the presence of calcium. Mixtures were centrifuged at 80 000 ***g***, 25 °C, for 15 min in a Beckman TL100 ultracentrifuge. Samples collected before and after centrifugation were analysed by SDS/PAGE.

Limited proteolysis and MALDI-TOF-MS

In the proteolysis experiments, 2 μg·mL^{-1} of the lyophilized chimera was dissolved in 10 mM ammonium bicarbonate solution pH 8.0, with the addition of 1 mM EDTA for the experiments in the absence of calcium or 1 mM $CaCl_2$ for the experiments in the presence of calcium. The lysis experiments were performed with 0.1 μg·mL^{-1} trypsin (Sigma, St. Louis, MO, USA) at 37 °C or at 4 °C and stopped by addition of a freshly prepared CHCA matrix solution (10 mg·mL^{-1}, H_2O/acetonitril/trifluoroacetic acid (3%) = 4/5/1, v/v/v) in time intervals of: 0, 15, 30, 45, 60, 120 and 180 min, and 24 h. The dried-doplet technique was used for MALDI-ToF-MS sample preparation. The mass spectra were recorded in both linear and reflection modes using a 4700 Proteomics Analyser (Applied Biosystems, Foster City, CA, USA) and mass ranges from *m/z* 400 to *m/z* 30 000 were observed. Each measurement consisted of 8–12 spectra, and the peptides were identified by their monoisotopic masses.

Small angle X-ray scattering experiments

Experiments were performed at the SAXS beamline of the Laboratório Nacional de Luz Síncrotron (LNLS) in Campinas, Brazil. The monochromatic beam was tuned at 8.33 KeV and the experimental setup included a temperature-controlled, 1 mm-thick sample cell with mica windows, and a linear position-sensitive detector. The samples at concentrations of 4–8 mg·mL^{-1} and in the same buffer conditions described for CD measurements were kept at 20 °C during the exposures and data acquisition was performed by taking five 900 s frames for each sample, allowing control of any possible radiation damage. The sample to detector distance was 445 mm, which enabled detection of a q range [$q = (4\pi/L)\sin(\theta)$, λ = wavelength and 2θ = scattering angle] equal to $0.025 \cdot Å^{-1} < q < 0.25 \cdot Å^{-1}$. Data analysis of the scattering intensities was performed using the software package TRAT1D [36] using the usual correction for detector homogeneity, incident beam intensity, sample absorption, blank subtraction and intensity averaging. Data

analysis and model calculations were performed using the computer programs GNOM [37], GASBOR [38], CHADD [39], and HYDROPRO [40]. Curve-fitting and desmearing of the experimental data was done using the GNOM software package [37]. From the program fitted curve the inverse Fourier transform from the scattering intensity was calculated. The resulting pair distance distribution function p(r) went to zero for the *r*-value corresponding to the particle maximum dimension D_{max}. The second moment of the p(r) function, equal to the radius of gyration R_g of the scattering particle, was also calculated. We also calculated the so-called Kratky plots ($I.q^2 \times q^2$) which give information on the compactness of the protein structure. The Kratky plots show a well-defined curve with an initial upward portion followed by a descending bell-shaped curve for particles with compact shape and without flexible domains, and a characteristic plateau and a monotonic rise at higher angles for particles with random coil conformation. Structured particles with flexible domains will have a well-defined maximum but with a descending curve that does not reach the horizontal axis [41].

Ab initio calculations were performed to obtain model structures. There are several methods for model calculations [38,39,42] and the choice of the right method depends on the experimental data. However, for all methods, the major problem is that SAXS is a low-resolution and low-information technique, which renders nonunique solutions. Increasing the measured q-range and imposing some shape and/or symmetry constraints can reduce the redundancy of the models [17]. The information from the structure of TnC(1–91) (1SKT) was used to produce domain structure models from solution scattering data from TnC(1–91)–TnI(1–182) and TnC(1–91)–TnI(98–147), following the strategies outlined by Petoukov and coworkers [39]. In this approach, the polypeptide chains are represented by fictitious amino acid residues centred at the Cα atomic positions. The separation of the residues in the molecular structure is smaller than the resolution of the scattering experiments (≈ 0.5 nm). Consequently, the protein chains can be modelled as an assembly of dummy residues. The program CHADD was used to attach a dummy backbone composed of the desired number of dummy residues to the backbone of the TnC(1–91), at position 91. In the case of the TnC(1–91)–TnI(98–182) model simulation, the number of dummy residues attached was 90, and for the TnC(1–91)–TnI(98–147) model simulation 55 dummy residues were attached. In the simulation process, a grid of water atoms was placed around the model to mimic the hydration layer of the protein in solution. Using a simulated annealing optimization, the program searches the best configuration of the attached backbone that gives the minimum discrepancy between the calculated scattering intensity from the *ab initio* model and the experimental SAXS data. Using this methodology, the available search space for the model configuration is reduced because of the constraints imposed on its conformation, consequently reducing the model redundancy. As a result of these calculations, the final dummy backbone conformation represented the linker and TnI components of the chimeras. In order to retrieve the most probable configuration, an average of the *ab initio* models was obtained using the program DAMAVER [43]. In this procedure the models were compared to each other by the alignment program SUBCOMP [44] and the models that had higher similarity were averaged. The most probable configuration was space-filled with a close packing of spheres. In each case we calculated 10 independent models and we found very good fits with $\chi^2 < 0.7$ (data not shown).

Acknowledgements

The authors thank the PEW Charitable Trust, the Fundação de Amparo à Pesquisa do Estado de São Paulo (FAPESP), and the Conselho Nacional de Desenvolvimento Científico e Tecnológico (CNPq) for financial support. A.O.T. is a CNPq fellow and L.T. and C.L.P.O. are FAPESP fellows. We also thank Dr A. Spisni for helpful discussions and the technical staff at LNLS for valuable assistance.

References

1 Farah CS & Reinach FC (1995) The troponin complex and regulation of muscle contraction. *FASEB J* **9**, 755–767.
2 Gordon AM, Homsher E & Regnier M (2000) Regulation of contraction in striated muscle. *Physiol Rev* **80**, 853–924.
3 Potter JD & Gergely J (1975) The calcium and magnesium binding sites on troponin and their role in the regulation of myofibrillar adenosine triphosphatase. *J Biol Chem* **250**, 4628–4633.
4 Zot HJ & Potter JD (1982) A structural role for the Ca^{2+}-Mg^{2+} sites on troponin C in the regulation of muscle contraction. Preparation and properties of troponin C depleted myofibrils. *J Biol Chem* **257**, 7678–7683.
5 Syska H, Wilkinson JM, Grand RJA & Perry SV (1976) The relationship between biological activity and primary structure of troponin I from white skeletal muscle of the rabbit. *Biochem J* **153**, 375–387.
6 Herzberg O & James MN (1985) Structure of the calcium regulatory muscle protein troponin-C at 28 A resolution. *Nature* **313**, 653–659.
7 Johnson JD, Charlton SC & Potter JD (1979) A fluorescence stopped flow analysis of Ca^{2+} exchange with troponin C. *J Biol Chem* **254**, 3497–3502.
8 Li MX, Chandra M, Pearlstone JR, Racher KI, Trigo-Gonzalez G, Borgford T, Kay CM & Smillie LB (1994) Properties of isolated recombinant N and C domains of chicken troponin C. *Biochemistry* **33**, 917–925.

9 Gagne SM, Tsuda S, Li MX, Smillie LB & Sykes BD (1995) Structures of the troponin C regulatory domains in the apo and calcium- saturated states. *Nat Struct Biol* **2**, 784–789.
10 Farah CS, Miyamoto CA, Ramos CHI, Silva ACR, Quaggio RB, Fujimori K, Smillie LB & Reinach FC (1994) Structural and regulatory functions of the NH2- and COOH-terminal regions of skeletal muscle troponin I. *J Biol Chem* **269**, 5230–5240.
11 Kobayashi T, Tao T, Gergely J & Collins JH (1994) Structure of the troponin complex. Implications of photocross-linking of troponin I to troponin C thiol mutants. *J Biol Chem* **269**, 5725–5729.
12 McKay RT, Tripet BP, Hodges RS & Sykes BD (1997) Interaction of the second binding region of troponin I with the regulatory domain of skeletal muscle troponin C as determined by NMR spectroscopy. *J Biol Chem* **272**, 28494–28500.
13 Pearlstone JR, Sykes BD & Smillie LB (1997) Interactions of structural C and regulatory N domains of troponin C with repeated sequence motifs in troponin I. *Biochemistry* **36**, 7601–7606.
14 Takeda S, Kobayashi T, Taniguchi H, Hayashi H & Maeda Y (1997) Structural and functional domains of the troponin complex revealed by limited digestion. *Eur J Biochem* **246**, 611–617.
15 Tripet B, VanEik JE & Hodges RS (1997) Mapping of a second actin-tropomyosin and a second troponin C binding site within the C terminus of troponin I, and their importance in the Ca^{2+}-dependent regulation of muscle contraction. *J Mol Biol* **271**, 728–750.
16 Ramos CHI (1999) Mapping subdomains in the C-terminal region of troponin I involved in its binding to troponin C and to thin filament. *J Biol Chem* **274**, 18189–18195.
17 Olah GA & Trewhella J (1994) A model structure of the muscle protein complex $4Ca^{2+}$.troponin C.troponin I derived from small-angle scattering data: implications for regulation. *Biochemistry* **33**, 12800–12806.
18 Stone DB, Timmins PA, Schneider DK, Krylova I, Ramos CHI, Reinach FC & Mendelson RA (1998) The effect of regulatory Ca2+ on the in situ structures of troponin C and troponin I: a neutron scattering study. *J Mol Biol* **281**, 689–704.
19 McKay RT, Pearlstone JR, Corson DC, Gagne SM, Smillie LB & Sykes BD (1998) Structure and interaction site of the regulatory domain of troponin-C when complexed with the 96–148 region of troponin-I. *Biochemistry* **37**, 12419–12430.
20 Takeda S, Yamashita A, Maeda K & Maeda Y (2003) Structure of the core domain of human cardiac troponin in the Ca (2+)-saturated form. *Nature* **424**, 35–41.
21 Ramos CHI, Lima MV Jr, Silva SL, Borin PFL, Régis WCB & Santoro MM (2004) Stability and folding studies of the N-domain of troponin C. Evidence for the formation of an intermediate. *Arch Biochem Biophys* **427**, 135–142.
22 Svergun DI, Barberato C & Koch MHJ (1995) CRYSOL: a program to evaluate X-ray solution scattering of biological macromolecules from atomic coordinates. *J Appl Cryst* **28**, 768–773.
23 Gralle M, Botelho MM, Oliveira CLP, Torriani I & Ferreira ST (2002) Solution studies and structural model of the extracellular domain of human amyloid precursor protein. *Biophys J* **83**, 3513–3524.
24 Borges JC, Hannes F, Craievich AF, Hansen LD & Ramos CHI (2003) Free human mitochondrial GrpE is a symmetric dimer in solution. *J Biol Chem* **278**, 35337–35344.
25 Chou WC, Liao KW, Lo YC, Jiang SY, Yeh MY & Roffler SR (1999) Expression of chimeric monomer and dimer proteins on the plasma membrane of mammalian cells. *Biotechnol Bioeng* **65**, 160–169.
26 Meyer RD & Rahimi N (2003) Comparative structure-function analysis of VEGFR-1 and VEGFR-2: What have we learned from chimeric systems? *Ann NY Acad Sci* **995**, 200–207.
27 Rizzuto R, Brini M, Pizzo P, Murgia M & Pozzan T (1995) Chimeric green fluorescent protein as a tool for visualizing subcellular organelles in living cells. *Curr Biol* **5**, 635–642.
28 Shin SU & Morrison SL (1989) Production and properties of chimeric antibody molecules. *Methods Enzymol* **178**, 459–476.
29 Chamberlin SG, Brennan L, Puddicombe SM, Davies DE & Turner DL (2001) Solution structure of the mEGF/TGFalpha44–50 chimeric growth factor. *Eur J Biochem* **268**, 6247–6255.
30 Dey B, Del Castillo CS & Berger EA (2003) Neutralization of human immunodeficiency virus type 1 by sCD4-17b, a single-chain chimeric protein, based on sequential interaction of gp120 with CD4 and coreceptor. *J Virol* **77**, 2859–2865.
31 Fontana A, Fassina G, Vita C, Dalzoppo D, Zamai M & Zambonin M (1986) Correlation between sites of limited proteolysis and segmental mobility in thermolysin. *Biochemistry* **25**, 1847–1851.
32 Li Z, Gergely J & Tao T (2001) Proximity relationships between residue 117 of rabbit skeletal troponin-I and residues in troponin-C and actin. *Biophys J* **81**, 321–333.
33 Oliveira DC & Reinach FC (2003) The calcium-induced switch in the troponin complex probed by fluorescent mutants of troponin I. *Eur J Biochem* **270**, 2937–2944.
34 Lakowicz JR, Gryczynski I, Cheung HC, Wang CK, Johnson ML & Joshi N (1988) Distance distributions in proteins recovered by using frequency-domain fluorometry. Applications to troponin I and its complex with troponin C. *Biochemistry* **27**, 9149–9160.

35 Heinohen JK & Lahti RJ (1987) A new and convenient calorimetric determination of inorganic orthophosphate and its application to the assay of inorganic pyrophosphatase. *Anal Biochem* **113**, 313–317.
36 Oliveira CLP (2003) TRAT1D – Computer Program for SAXS Data Treatment. LNLS technical Manual MT 01/2003.
37 Semenyuk V & Svergun DI (1991) *GNOM* – a program package for small-angle scattering data processing. *J Appl Crystal* **24**, 537–540.
38 Svergun DI, Petoukhov MV & Koch MHJ (2001) Determination of domain structure of proteins from X-ray solution scattering. *Biophys J* **80**, 2946–2953.
39 Petoukhov MV, Eady NAJ, Brown KA & Svergun DI (2002) Addition of missing loops and domains to protein models using X-ray solution scattering. *Biophys J* **83**, 3113–3125.
40 de la Torre JC, Huertas ML & Carrasco B (2000) Calculation of Hydrodynamic Properties of Globular Proteins from Their Atomic-level Structure. *Biophys J* **78**, 719–730.
41 Botelho MG, Gralle M, Oliveira CLP, Torriani IL & Ferreira ST (2003) Folding and stability of the extracellular domain of the human amyloid precursor protein. *J Biol Chem* **278**, 34259–34267.
42 Svergun DI (1999) Restoring low resolution structure of biological macromolecules from solution scattering using simulated annealing. *Biophys J* **76**, 2879–2886.
43 Svergun DI & Petoukhov MV (2003) DAMAVER – set of programs to align the models provided by DAMMIN and GASBOR and to build 'the most probable' model – beta version, http://www.embl-hamburg.de/ExternalInfo/Research/Sax/damaver.html
44 Kozin MB & Svergun DI (2001) Automated matching of high- and low-resolution structural models. *J Appl Cryst* **34**, 33–41.